

Universal Scale Laws for Colors and Patterns in Imagery

RÉMI MICHEL^{1,*} AND MOHAMED TAMAZOUSTI¹

¹Université Paris-Saclay, CEA, List, F-91120, Palaiseau, France

*remi.michel@cea.fr

Abstract: Distribution of colors and patterns in images is observed through cascades that adjust spatial resolution and dynamics. Cascades of colors reveal the emergent universal property that Fully Colored Images (FCIs) of natural scenes adhere to the debated continuous linear log-scale law (slope -2.00 ± 0.01) (L1). Cascades of discrete 2×2 patterns are derived from pixel squares reductions onto the seven unlabeled rotation-free textures (0000, 0001, 0011, 0012, 0101, 0102, 0123). They exhibit an unparalleled universal entropy maximum of 1.74 ± 0.013 at some dynamics regardless of spatial scale (L2). Patterns also adhere to the Integral Fluctuation Theorem (1.00 ± 0.01) (L3), pivotal in studies of chaotic systems. Images with fewer colors exhibit quadratic shift and bias from L1 and L3 but adhere to L2. Randomized Hilbert fractals FCIs better match the laws than basic-to-AI-based simulations. Those results are of interest in Neural Networks, out of equilibrium physics and spectral imagery.

1. Introduction

Images (B&W, RGB or multi-spectral) offer a never ending tricky composition of colored pixels [1–6]. Their interpretation is of major interest in thematic imagery [7, 8], in statistical physics [9, 10] and in image processing [11, 12]. Universal behaviors derived from images are of key interest because they allow to derive parameters of physical models and to put constraints on numerical models. Among them are the so-called scaling laws showing near fractal organisation of discrete patterns and the celebrated $1/f^\alpha$ densities in the continuous domain [13–16]. Discrete patterns, textures, and local Hamiltonians of physical systems also exhibit universality, as seen with Potts models [17] or with fluctuations of entropy across scales, which are notable in both image theory and physics [18–24]. Numerous mathematical tools and theories in the field take benefit of those general behaviors, including Fourier descriptors, texture analysis, Wavelets [25], Local Binary Patterns [26, 27] and Markov random fields. These laws appear in the study of the deep neural networks which process those images [28]. They serve as valuable features for the data (including images) or for the internal representation of learning machines [29]. They are more generally of interest in a variety of domains [30–32]. But as of today, the origin of those scaling laws and the compliance of acquired images with them is still an open debate [5, 33]. In this paper we propose an investigation of universal color and spatial structures in images of natural scenes based on three main remarks. The first remark is that patterns in images change with exposure time and sensitivity of recorders. This arises from the quantization and noise. A second remark is about the geometry of patterns. We basically choose the geometry of 2×2 square pattern because it's the most basic 2D pattern equally suitable for texture analysis, local Hamiltonian of physics and fractals. A latest remark is that patterns are conceptual. We thus choose the most basic rule to transform measurements using an unlabelled pattern descriptor that provides the same (resp. different) value at pixels which values σ_i equal (resp. differ). Contrast invariant descriptors are unlabelled. Such unlabelled patterns also occur in statistical physics; the Ising (or Potts) Hamiltonian $H_i = -J \sum_{j \in V(i)} \delta(\sigma_i, \sigma_j)$ yields a 5 levels Hamiltonian from unlabelled comparison between σ_i and σ_j . The delta occurs from the Pauli exclusion principle in that case and we do not have such a principle in imagery. Thus we can not assign energy levels to patterns without assumptions. Thermodynamical models based on the assumption of the Ising models have been proposed that provide multi-scale descriptions of binarized representation

of images [5, 16, 34–38]. Following those studies, we propose to identify universal constants regarding colors and patterns in images of natural scenes. This will be based on a procedure that systematically captures spatial resolution and dynamics but without presuppositions about the energy levels of patterns.








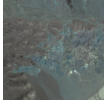


In the following, we first present a database of images im and introduce the Fully Colored Images. We then present a cascade C derived from im that allows to grasp the variations of patterns with dynamics and spatial scale. A local 2×2 7-states texture patterns basis is derived from an Ising-like local Hamiltonian and the cascade is transformed into a cascade H of the patterns describing local textures. Results describe statistics of cascades C and H through the notion of Shannon’s entropy. The discussion encompasses power laws (continuous and discrete), the integral fluctuation of entropies with spatial scale and fractality through comparison with models.

2. Method

2.1. Spectral Images

Images used in this study are multi-channels images of various contexts, cropped by square of $N \times N = 256 \times 256$ pixels, the number of spectral channels varies from 1 (B&W images) to 32 and includes standard RGB 3-channels images (Table 1). Typically all pixels differ in images of natural scenes 256×256 that have a dynamics of 1 octets or more and 3-5 or more independent spectral channels; we refer to them as Fully Colored Images (FCI). RGB images used in this study include more than 97% of distinct colors (Table 1). It’s worth noting that any natural scene can potentially be captured as FCI ; it solely depends on the camera, including its dynamics and spectral channels.

Table 1. Databases [39–41] of RGB and Multi-spectral Images (256×256 pixels). Percentage of independent colors typically close to 100% (Fully Colored Images) for {dynamics>256, Channels>3}.

Dyn	256	256	256	300	300
Channels	3	3	5	32	32
Colors (%)	94	95	100	100	100
Ref	Baboon	Face	Flower	Foster1	Foster2
IMAGE					
Dyn	300	300	300	300	310
Channels	32	32	32	32	32
Colors (%)	100	100	100	100	100
Ref	Valley	Fern	Cuprite	Hyperion1	Hyperion2
IMAGE					

2.2. Cascade $C(k, s)$ of Spectral Images

In order to grasp most information included in images we choose to analyse them at various spatial scales and dynamics through the cascade of images $C(k, s)$

$$C(k, s) = [im * g(s)]_{\downarrow} / k \quad (1)$$

where $/$ denotes euclidean division, $*$ denotes convolution, k is integer in the range $[0, k_{\max} = \max(im) + 1]$, $g(s)$ is a top at $s \times s$ normalized window and \downarrow denotes sub-sampling by a factor s . $C(1, 1)$ is im and $C(k_{\max}, s)$ are black images, noted $[0]$ hereafter (see Fig. 1).

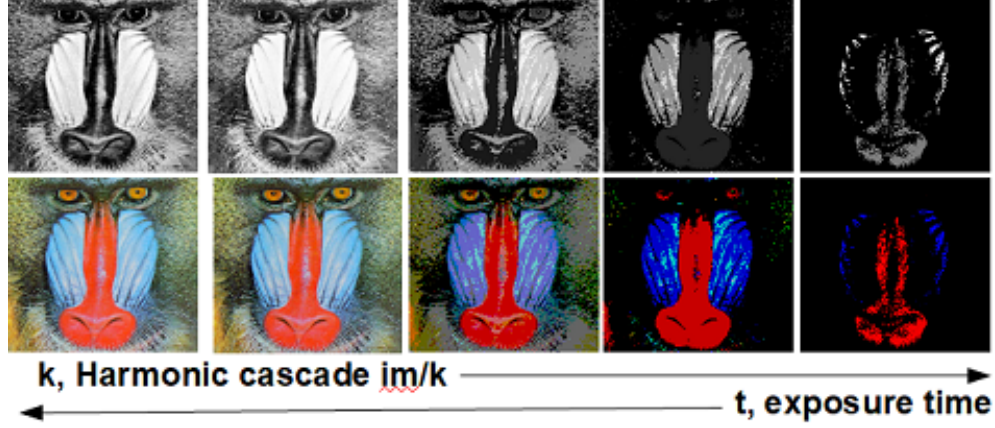


Fig. 1. Bottom: Patterns appear during exposure time, cascade $C(k, 1) = im/k$. Top : flag of independent colors in levels of grey. Bottom : im/k , rescaled to 1 octet

2.3. Local 2×2 Hamiltonian and Patterns

At point M of an image im , we define the local texture from the hamiltonian $H_{im}(M)$:

$$H_{im}(M) = \sum_{(i,j) \in V(M)} \frac{\delta(\sigma_i, \sigma_j)}{d(i, j)} \quad (2)$$

where V is the 2×2 square including M at bottom left and $d(i, j)$ the euclidean distance. $H_{im}(M)$ is both unlabelled, through the comparison made by the δ function, and invariant per rotation of the 4 pixels in $V(M)$. For each loop of 4 colored (spectral) pixels $H_{im}(M)$ can take 7 distinct values. $H_{im}(M)$ reduces each spectral loop to its class of equivalence in the set of the 7 unlabelled necklaces that have minimum lexicographic representatives 0000, 0001, 0011, 0012, 0101, 0102, 0123. $H_{im}(M)$ thus describes the local structure (or local texture) and those 7 patterns constitute the basis of patterns of the study (see Table 2).

Table 2. Local Patterns Basis. Each local loop of four pixels yields one of the 7 values H_i of the Hamiltonian representing the class of equivalence in the set of the 7 unlabeled necklaces (4, 4).

Local Pattern							
Unlabeled Necklace	0000	0001	0011	0012	0101	0102	0123

$H_{C(1,s)}$ nearly equals [0] because high spatial frequency variations of σ_i in images reduces most spectral loops 2×2 to pattern 0123, $H_{FCI} = [0]$ because all σ_i differ and $H_{C(k_{max},s)} = 4 + 2\sqrt{2}$ because the null image always reduces to loops equivalent to 0000 (see Fig. 2).

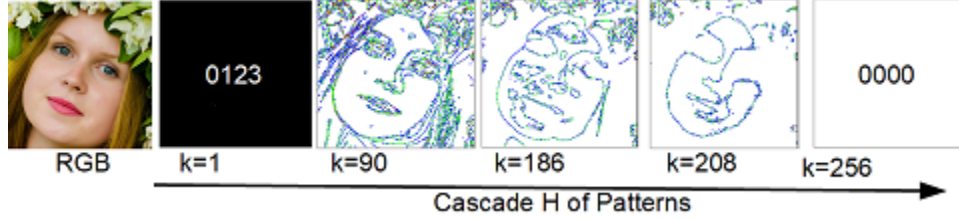


Fig. 2. Patterns evolution with k , cascade $C(k, 1) = \frac{im}{k}$ for the 7 patterns (arbitrary colors). At $k = 1$ in most images local patterns resume to 0123 because all local σ_i differ. For $k > \max(im)$, $C(k, 1) = [0]$ and patterns resume to 0000. In between, patterns fluctuate with universal maximum 1.74 ± 0.013 for Shannon entropy and at compliance with the Integral Fluctuation Theorem for entropy production over scales (see text for details). Original image (left) from database [41].

3. Results

3.1. Log-scale Entropy of Fully Colored Images

The Shannon entropy of images is defined as:

$$S_{im} = - \sum_m p(m) \log(p(m)) \quad (3)$$

where m is the number of different σ_i in the image and $p(m)$ is the probability associated with σ_i . The entropy of the cascade S_C for varying values of k and s are presented in Fig. 3. The density of states (id. the histogram) of $C(k, s)$ is derived from that of $C(1, s)$ by binning the density of states by a step k . The entropy decreases with k , though not monotonically, is maximum for $k=1$ and zero at k_{max} .

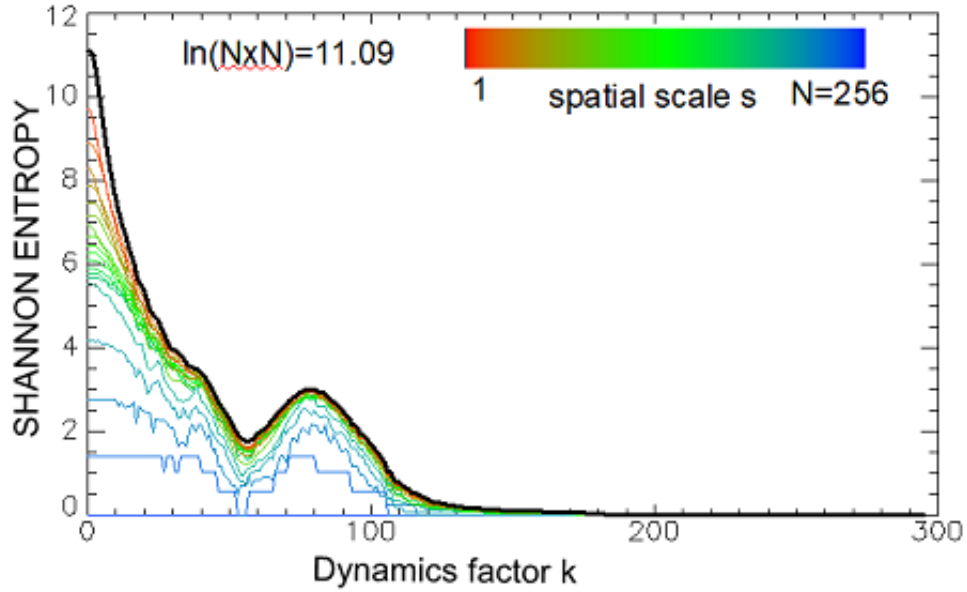


Fig. 3. Entropy S_C of $C(k, s)$. Cuprite image $(256 \times 256) \times 16$ channels, Fully Colored. S_{C_k} depends only on density of states of $C(1, s)$ by binning into factor k . It does not decrease monotonically with k which contributes to variations in patterns along the cascade.

Variations of entropies with scale s depends on the organisation of pixels in the image, The entropies vary in a near linear log-scale law (Fig. 4). The greater the Shannon entropy of im , the more linear the decrease. The variations of the entropy with scale s shows that FCI have a universal log-linear variation with spatial scale s :

$$S_{FCI}(s) = -2 \log\left(\frac{s}{N}\right) \pm 0.01 \quad (4)$$

, thus validating for FCI the $1/f^2$ law [42]. When the image is not FCI than standard deviations on the estimates of the two coefficients of the best least-square linear fit increases, (see Fig. 5).

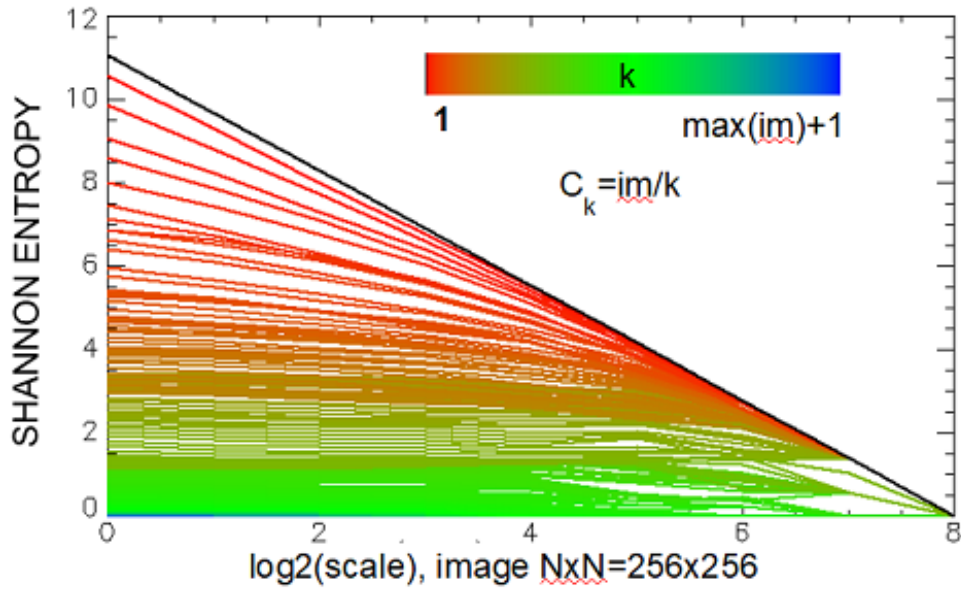


Fig. 4. Entropy S_C of the cascade (k, s) . Hyperion image $(256 \times 256) \times 32$ channels, Fully Colored. The linear Law is universal for Fully Colored Images (black line). A lower entropy, curvature at high resolution (low s) and bias at low resolution (high s).

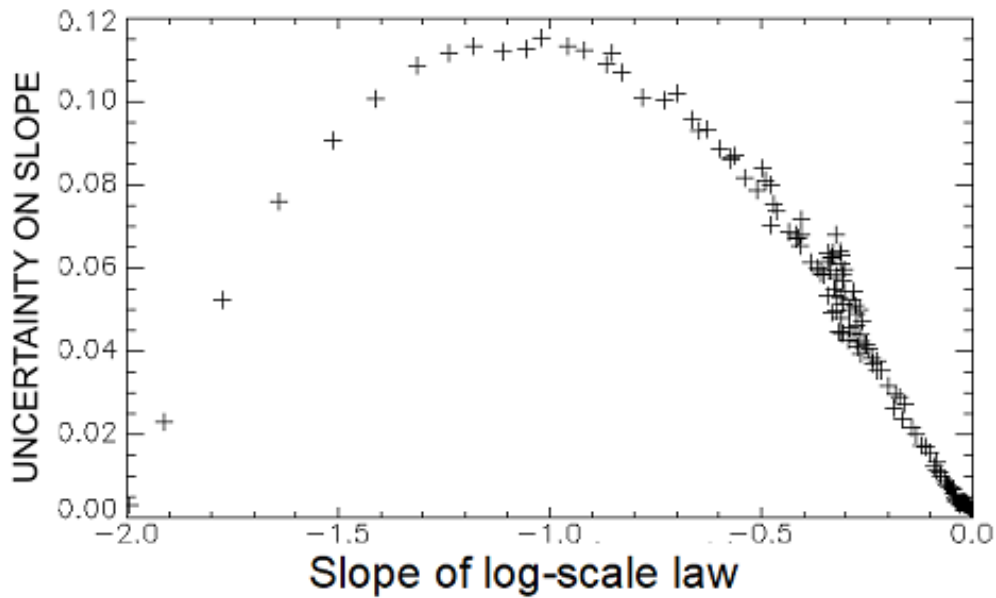


Fig. 5. Shift to $\log(s)$ as a Entropy of $C(k, s = 1)$ with k . Cuprite image $(256 \times 256) \times 8$, Fully Colored. FCI images (bottom left), are perfectly linear with slope $a = -2$ while best linear match at lower entropy of im reveals higher order contributions, when the image is near zero, both a and its standard deviation tends to zero.

3.2. Entropy of patterns

For any image $S_{H[C(k_{max},s)]} = 0$ because $C(k_{max},s) = [0]$, for most images $S_{H[C(1,1)]}$ is closed to zero as pattern 0123 dominates in textured images and $S_{H[FCI]} = 0$. In between, for varying values of k in the harmonics cascade, $S_{H(FCI)}$ presents an universal maximum equals to 1.74 ± 0.013 at each spatial scale, below the maximum $\ln(7) = 1.93$ (see Fig. 6 and Fig. 7).

$$\max_k [S_{H(FCI)}] = 1.74 \pm 0.013 \quad (5)$$

$$\frac{\partial}{\partial s} \max_k [S_{H(FCI)}] = 0 \quad (6)$$

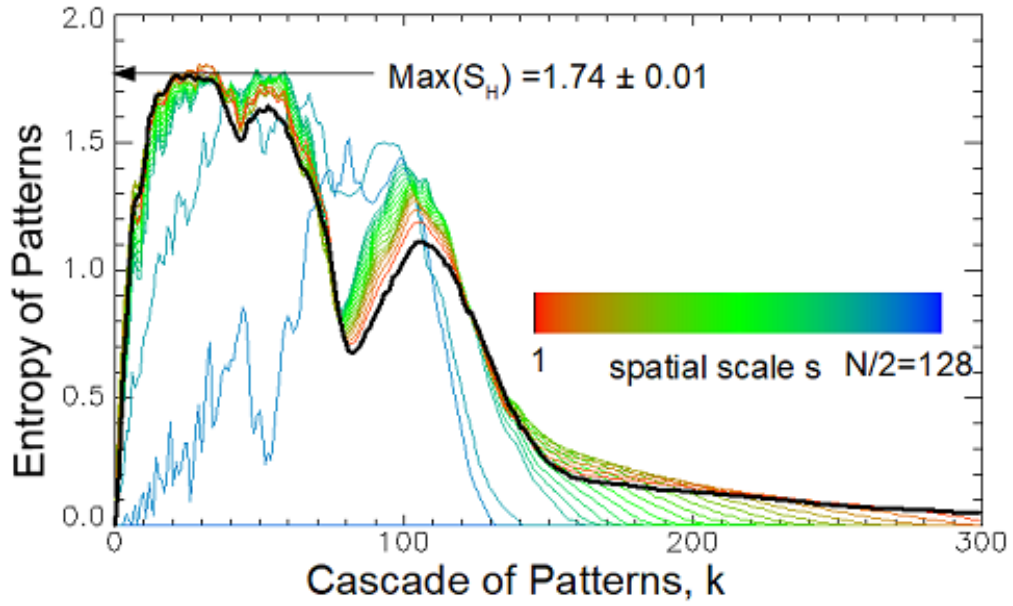


Fig. 6. Entropy of $H(C)$, 7 states. Universal Maximum of Entropy of patterns $S_H=1.74 \pm 0.013$, constant with scales for Fully Colored Images, below the maximum $\ln(7)$. Hyperion image $(256 \times 256) \times 32$ channels, Fully Colored (Hyperion 1)

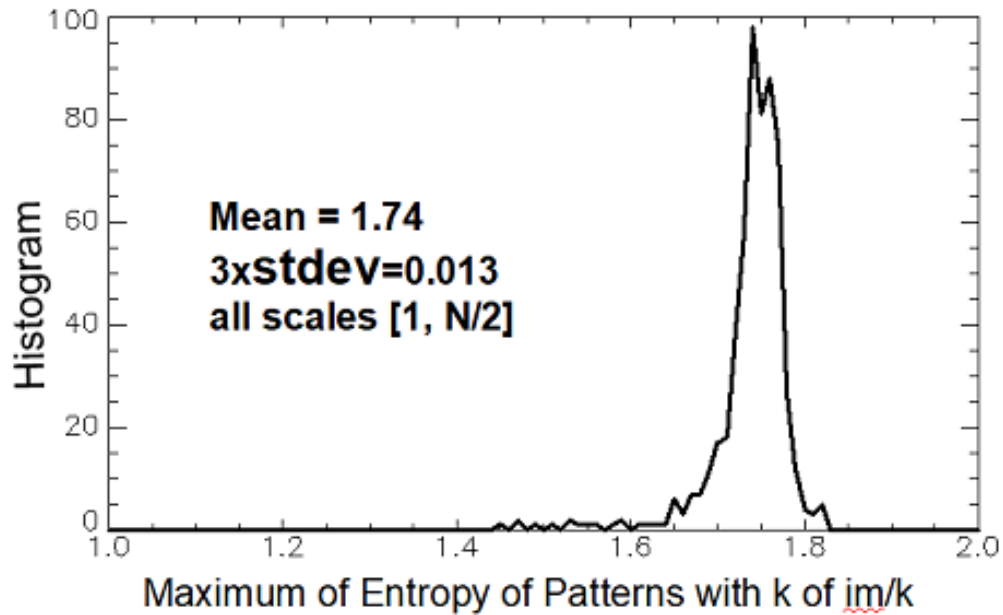


Fig. 7. Maximum of Entropy of $H(C)$ over database. Universal Maximum of entropy $S_H=1.74 \pm 0.01$, constant over scale for Fully Colored Images. Below $\ln(7)$, this maximum is interpreted as resulting from the scarcity of patterns 0101 and 0102 in images of natural scenes.

The entropy production varies smoothly with scales along the cascade at rates changing with the level k (see Fig. 8). Those variations resemble that reported for the complex dynamics of physical systems such as turbulent cascade in fluid dynamics, a domain where entropy production and transfer with scale is of paramount importance [23, 43].

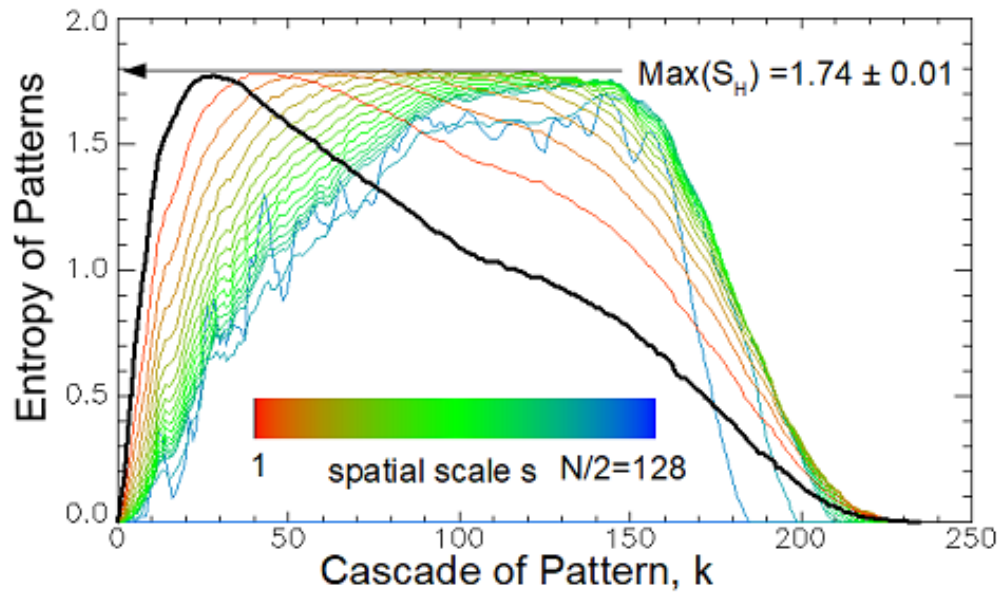


Fig. 8. Entropy of $H(C)$. The production of Entropy varies smoothly with scale (from black, red to deep blue) at depends on k . Flower image $(256 \times 256) \times 5$ channels, Fully Colored.

A trade-off between $\log(s)$ law and patterns distribution is noticeable in images that are far from being *FCI* (see Fig. 9). In that case, important shifts in the $\log(s)$ law occur while the maximum of the entropy of pattern is maintain.

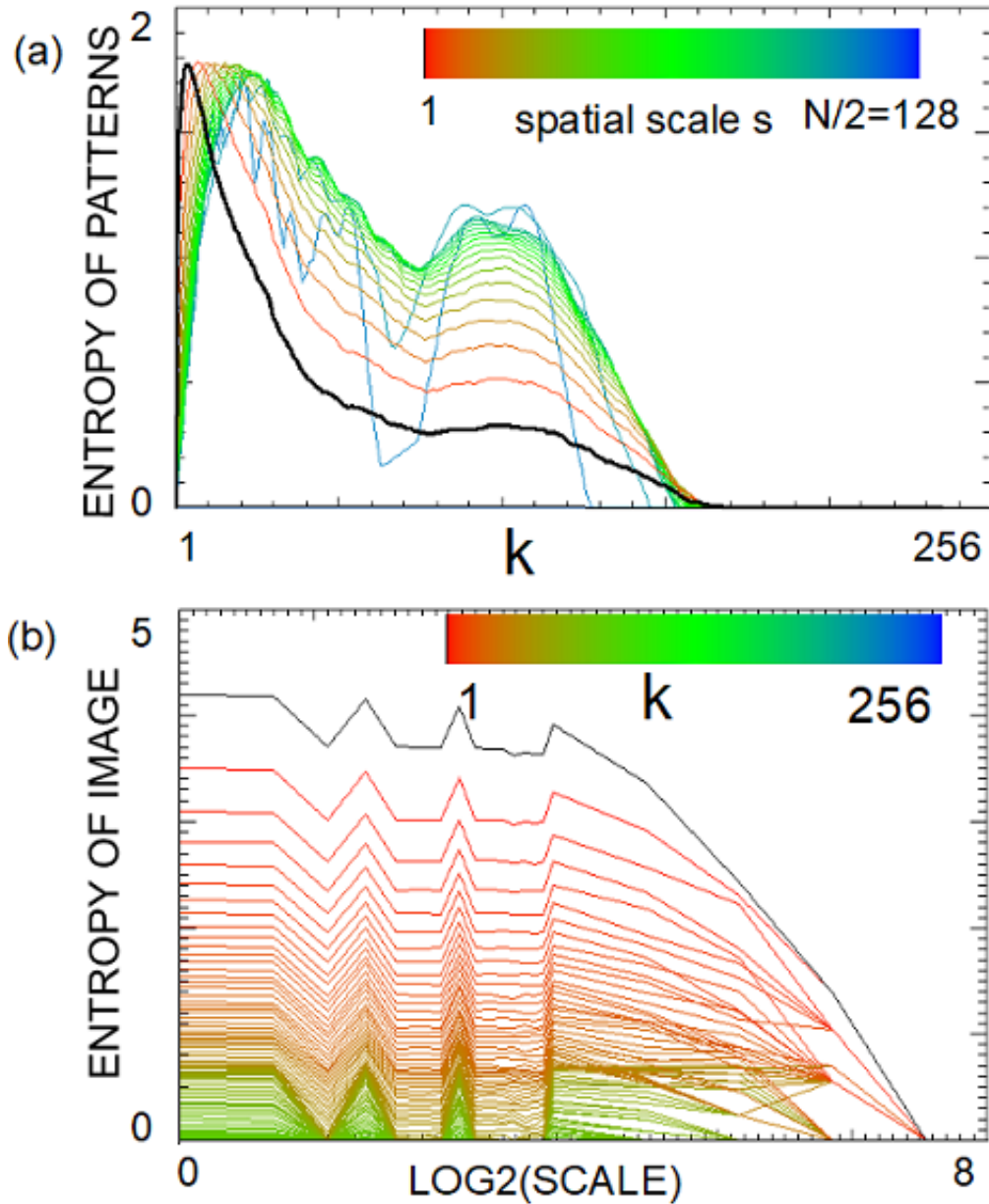


Fig. 9. Non *FCI* images of Natural Scene (Flower image ($256 \times 256 \times 2$) channels) tend to maintain $\max_k(S_H) = 1.74$ though they do not respect log-scale linearity.

3.3. Entropy Production and Integral Fluctuation Theorem for Natural Scene

The total production of entropy $\Omega_{\pm}(im)$ as a function of the spatial scale s (s being an integer) is defined as

$$\Omega_{\pm}(im) = \frac{1}{(N-1)} \sum_{s=1}^{N-1} \exp \pm \Delta S_{im}(s+1, s) \quad (7)$$

$\Delta S_{im}(s+1, s)$ is the difference of Shannon entropies S_{im} at spatial scales $s+1$ and s . $\Omega_{\pm}(C_k)$ fluctuates over k with values typically in the range $[0.5, 1.8]$ (see Fig. 10).

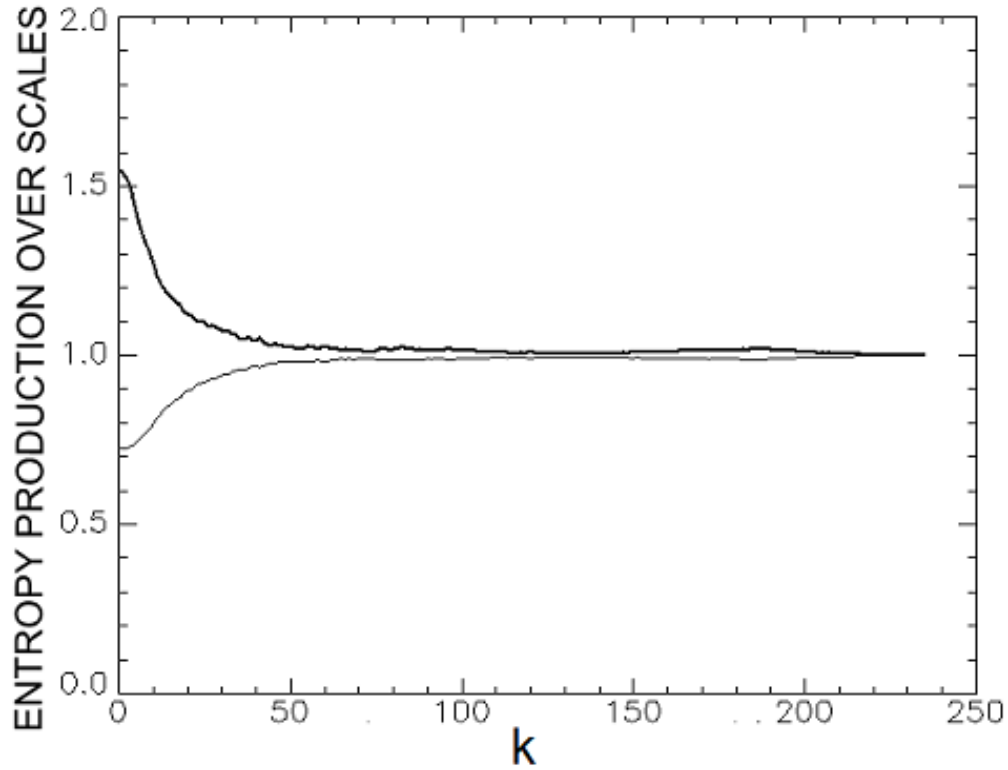


Fig. 10. Entropy Production of Image with scale of C (direct bold). Entropy production is balanced (grey) but does not respect the Integral Fluctuation Theorem. Hyperion image $(256 \times 256) \times 32$ channels, Fully Colored.

Because the pattern is 2×2 , the production $\Omega_{\pm}(H)$ of the Hamiltonian H describing local structures is limited in scale to $N/2$:

$$\Omega_{\pm}(H) = \frac{1}{(N/2 - 1)} \sum_{s=1}^{N/2} \exp \pm \Delta S_H(s + 1, s) \quad (8)$$

For FCI we get, for all values of k in the harmonic cascade (see Fig. 11):

$$\Omega_{\pm}(H) = 1.00 \pm 0.01 \quad (9)$$

Those values respect the so-called Integral Fluctuation Theorem and denote a hallmark of chaotic cascade that behave far from equilibrium. This property holds for all values of k in the cascade of FCI (see Fig. 11). At some values of k , $\Omega_{\pm}(H) = 1.00 \pm 1e^{-6}$, images presents balanced equilibrium with the maximum achievable accuracy in our context.

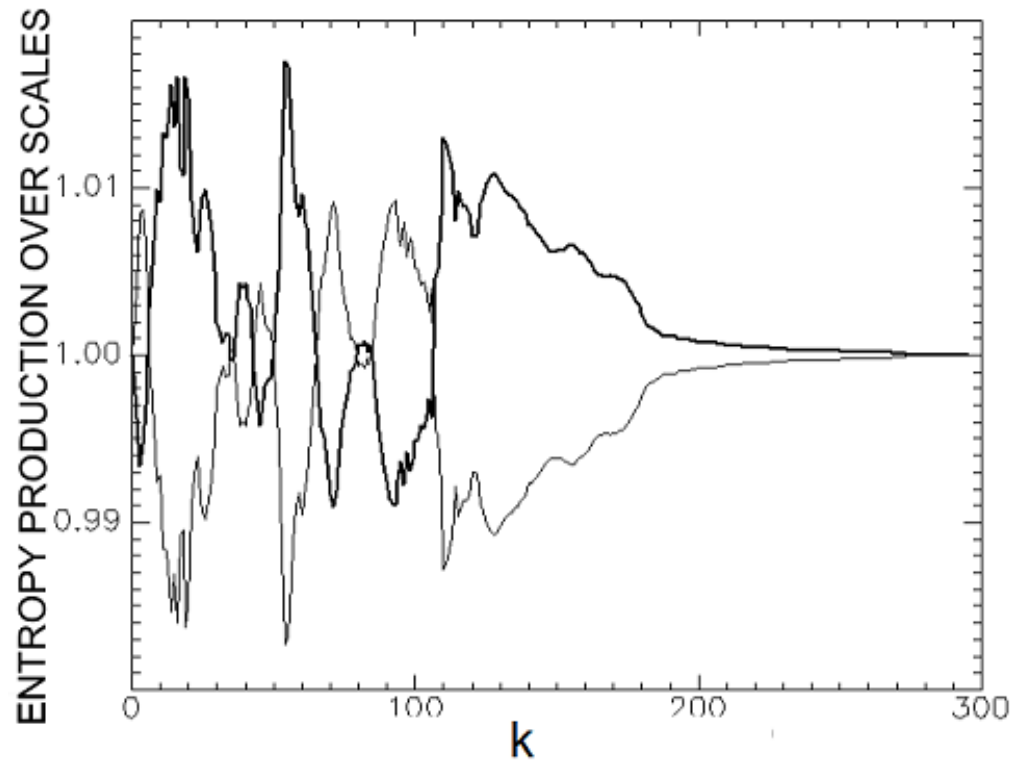


Fig. 11. Entropy Production with scale of Patterns follows the celebrated Integral Fluctuation Theorem (*IFT*) within ± 0.01 for all Natural Scenes. At some values of k , exact *IFT* is achieved. Cuprite image (256×256) \times 16 channels, Fully Colored.

When the images are not *FCI*, the values of the entropy production with scale do not shift from 1 with k (Fig. 12). supporting the assumption that the hamiltonian maintains the complexity of patterns with scale despite the log-scale law does not hold anymore.

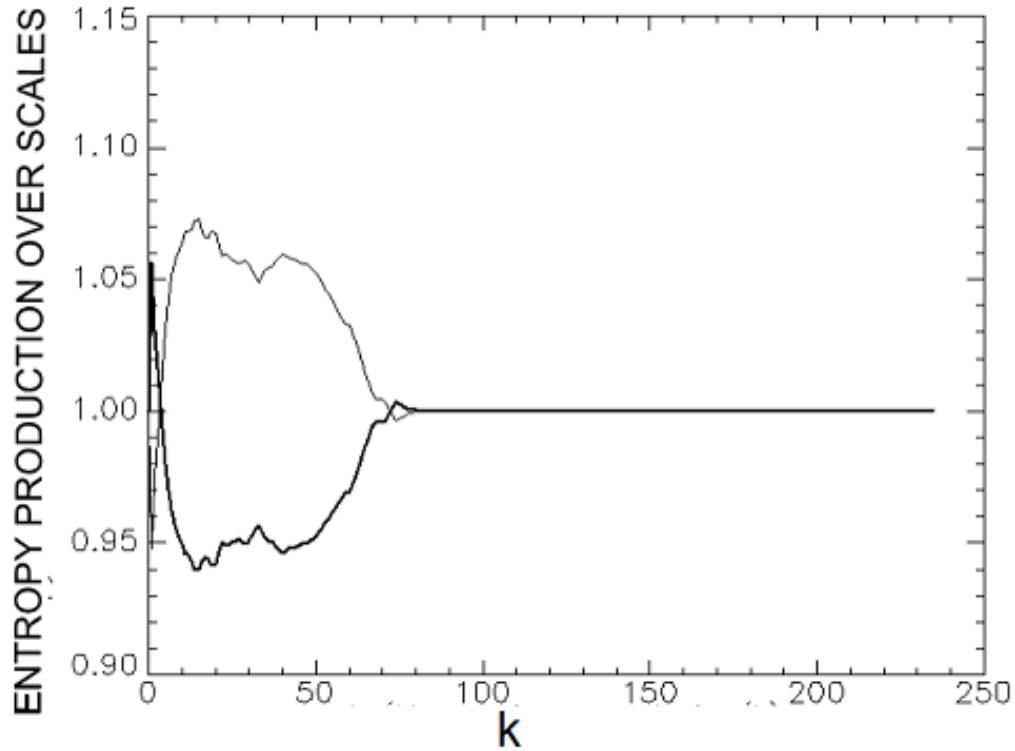


Fig. 12. Entropy Production of Patterns with scale in images of natural scenes far from being FCI is maintains. Flower image $(256 \times 256) \times 2$ channels.

4. Discussion

Simulating these three behaviors is far from a straightforward procedure. Such a complexity is particularly evident in domains dealing with intricate 2D (or higher-dimensional) systems. In the realm of image-oriented Artificial Intelligence, the convergence of super-resolution and the generation of fake images produces visually realistic and intricate patterns, making them ideal candidates for testing the proposed framework. Fields of physical phenomena that exhibit these behaviors include turbulence in fluid mechanics, non-equilibrium thermodynamics, biology, vision, finance and imagery [8, 44, 45]. In these domains, an history of studies has demonstrated the coherence between concepts such as fractal behavior, pattern orientation, the $1/f^\alpha$ spectral response of continuous models and Self-Organized Criticality [15, 46, 47]. The following simulations are inspired by those studies and aim at best reproduce the described behavior of images [48].

4.1. About the Scarcity of Some Patterns in Natural Scenes

The 7 patterns of this study, the Unlabelled Necklace (4,4), do not appear equally and pattern 0101 can hardly be found in images as shown with the integral of each pattern with k in the harmonic cascade (Fig. 13).

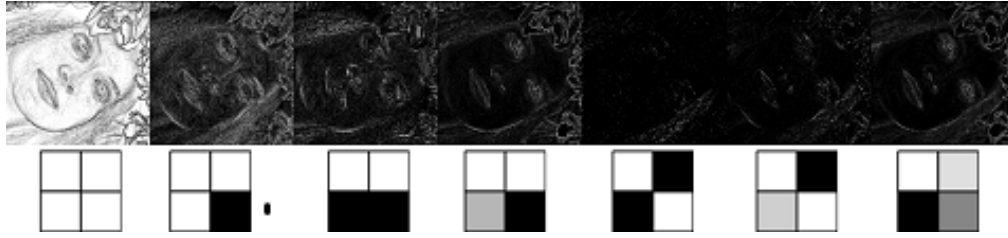


Fig. 13. Integral of each pattern with $k=1, s=1$, shows that 0101 and 0102 are the least present pattern in the field: **Relative Abundance (%)** : **71.77, 12.00, 7.09, 4.32, 0.55, 1.34, 2.92**.

We suggest that this scarcity results from the smoothness of natural patterns while information about smoothness is partially lost in the basic δ function of the hamiltonian of Eq. (2). A tile of the elevation of planet Earth as a single channel image shows high variations in the relative abundance of the 7 patterns; the scarcest, 0101, represents only 0.36% of patterns of the topographic tile and so mountain pass is the scarcest pattern in elevation at any scale (Table 3). This scarcity give insight why $\max_k [S_{H(\text{Plan})}] < \ln(7)$. The values H_i of the 7 necklaces from the hamiltonian of Eq. (2) do not provide direct incentive on how a physical model (e.g. a thermodynamical model with Boltzmann-like statistics) could recover this particular property at this step; adding an interaction with a to-be-defined external field that acts distinctly with the σ_i or other kind of models, like Self-Organized-Criticality may further help to describe results obtained in Table 3.

Table 3. Relative abundance of patterns in a Tile of the elevation of Earth (extracted from gtopo30 [49]) shows that necklace 0101 is the scarcest.

Pattern	0000	0001	0011	0012	0101	0102	0123
Occurrence (%)	80.9	8.1	4.7	2.9	0.36	0.96	2.0

4.2. Simulations

It's easy to construct images that present S_H greater than 1.74 and even equal to $\ln(7)$, just paving regularly the plane equally with the 7 patterns, those images just do not appear in natural scenes Table 4. Let's im be the most basic FCI plane $im(c, l) = c + l * N$. In order to reduce the

Table 4. Example of image with $S(H) = \ln 7$. First two lines repeatable *ad libitum*, new mirror columns may be added easily with different labels; all seven patterns always appear equally. This situation does not appear in natural scenes.

0	0	0	1	1	0	0	2
0	0	1	0	0	2	1	3
0	0	0	1	1	0	0	2
0	0	1	0	0	2	1	3

intractable dynamics N^2 of im and to mimic the correlation between spectral channels of images of natural scenes, we map monochromatic $N \times N$ images on the 2 channels FCI image with dynamics $2N$, $im(c, l, 0) = c + l$ and $im(c, l, 1) = N + c - l$. Results are presented in Fig. 14, this trivial FCI image respects the log-scale law but the value of the maximum of entropy, though

independent on the scale, only equals to

$$\max_k [S_{H(\text{Plan})}] = 1.05 \pm 0.01 \quad (10)$$

Such result was expected because of the low "complexity" of the plane but that case is still noticeable because it is opposite to that of Fig. 9 of a non fully colored natural scene that manage to respect $\max_k [S_{H(\text{Plan})}] = 1.74 \pm 0.01$ though not respecting the $\log(s)$ law.

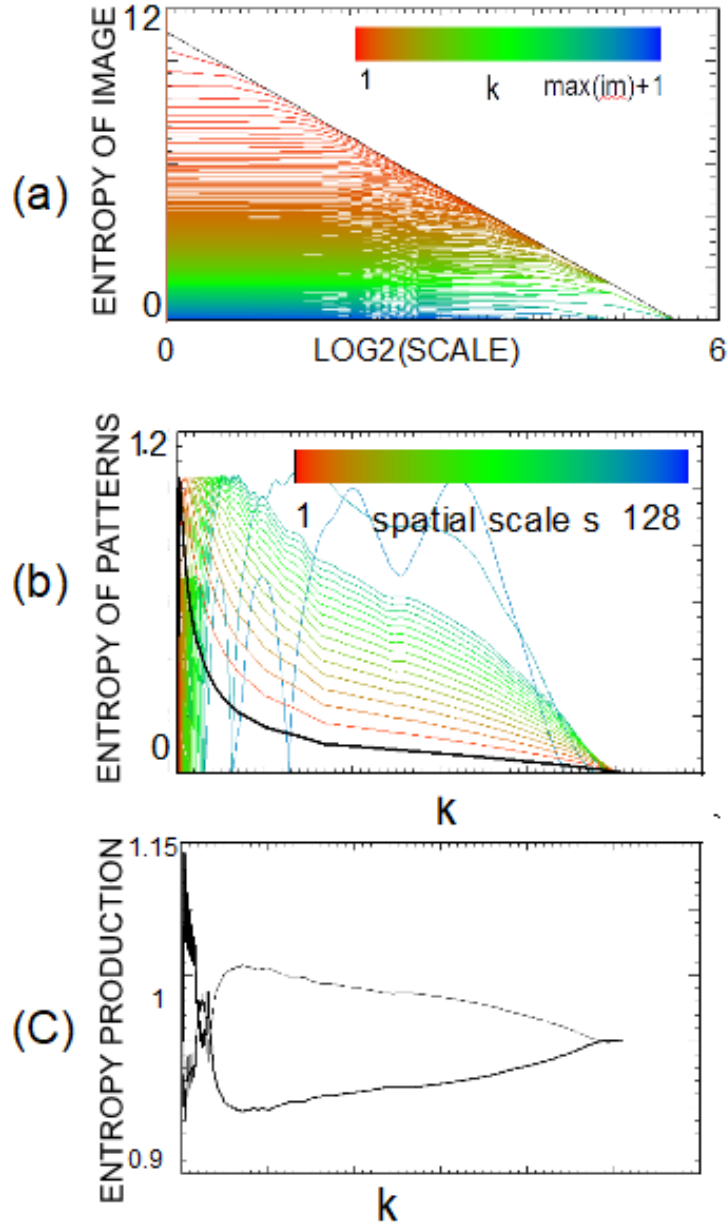


Fig. 14. Plane FCI ($256 \times 256 \times 2$ channels) respects log-scale (a) and balanced equilibrium (c) but yields $\max_k [S_{H(\text{Plan})}] = 1.05$. (b)

Hence we may infer that at low energy (high values of k in the harmonic cascade im/k) the image maintains the complexity of its organisation in term of patterns but not the log-scale law while basic models of *FCI* do the opposite. The same procedure has been used with a fully colored Random image $(N,N,2)$ with dynamic N that includes all the 2 spectrum located randomly. None of the three observations is respected, the log-scale law is highly biased, the maximum of entropy of pattern is 1.70 ± 0.01 and no balanced fluctuations (see Fig. 15).

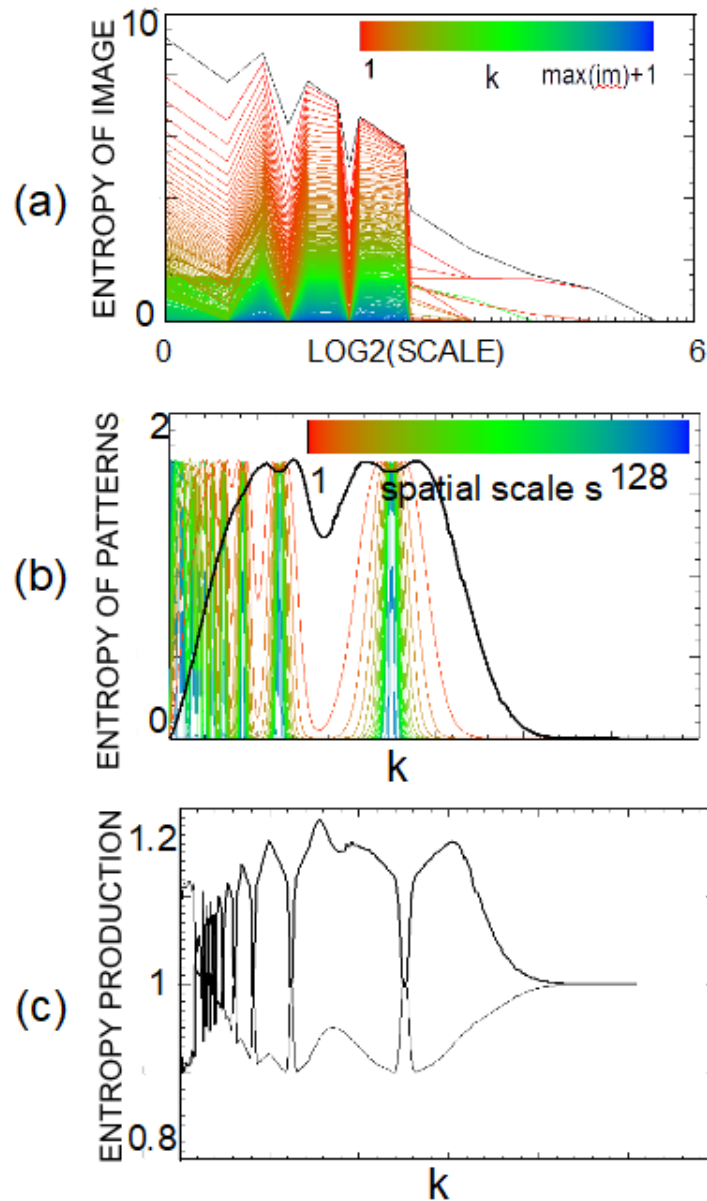


Fig. 15. Random FCI ($256 \times 256 \times 2$ channels) does not respect any of the 3 rules, log-scale (a) $\max_k [S_H(\text{Random})] = 1.70$ (b) and poorly balanced equilibrium (c) (see text).

Computer generated images [50] propose super-resolved images that include to few entropy at extrapolated scales $\times 2$ and stand below the log-scale law at interpolated scales s . Fakes build on statistically "melting" real faces better manage to respect all the three laws. The face image (see Table 1) reduced to 64×64 pixels and than super-resolved by a factor 4 by gets entropies at super-resolved scales $s = 1$ and $s = 2$ that are respectively 20% and 5% below the expected values for *FCI*, showing that the AI does not recover all of the details of the image [51]. A major inconvenient of those AI generated images for this study is that the process mainly transfer the complexity of images we want to grasp into the network (during training procedures). The neural networks may, when considered as graphs, exhibit similar properties than those described in this study especially when they are trained using images of natural scenes. Thus similar asymptotic laws may hold in the graphs which may be of help to better constrain their design. Fractal distribution of pattern has been studied and proposed for modeling of stochastic 2D process showing the relationship between $1/f$ and fractals [15]. In the context of the proposed 2×2 Hamiltonian and the requirement of a *FCI*, the Hilbert fractal of the 2×2 pattern 0123 allows to provide a Fully Colored Image that presents the pattern 0123 everywhere at any spatial scale s : At step 0 the square image is divided in $4 N/2 \times N/2$ sub-squares that are attributed a 2×2 permutation σ_i^0 of the vector $[0, 1, 2, 3]$. The iterative process in j consist in replacing each square σ_i^j by four sub-squares with new values:

$$\{\sigma_i^{j+1}\} = 4 * \sigma_i^j + P_j \quad (11)$$

where $\{.\}$ denotes the set of 4 news values and P_j a permutation of $[0,1,2,3]$. During the iterative process building the fractal we choose randomly the permutation P_j to get a randomized Hilbert fractal f . The fractal includes all integers between 0 and $N^2 - 1$ by construction. It is thus a *FCI* at any spatial scale s . The image is then mapped on a 2 channels Fully Colored Image of dynamics $2N$:

$$Fractal(i, 0) = \frac{f(i)}{N} + f(i) \quad \text{mod } N \quad (12)$$

$$Fractal(i, 1) = N + \frac{f(i)}{N} - f(i) \quad \text{mod } N \quad (13)$$

Modified Hilbert Fractals FCI ($256 \times 256 \times 2$ channels, dynamics $2N$) best fit the three laws. Randomness in the angle of rotation of the Hilbert 2×2 0123 pattern allows for a better fit of pattern entropy and a more accurately balanced entropy production, see Fig. 16.

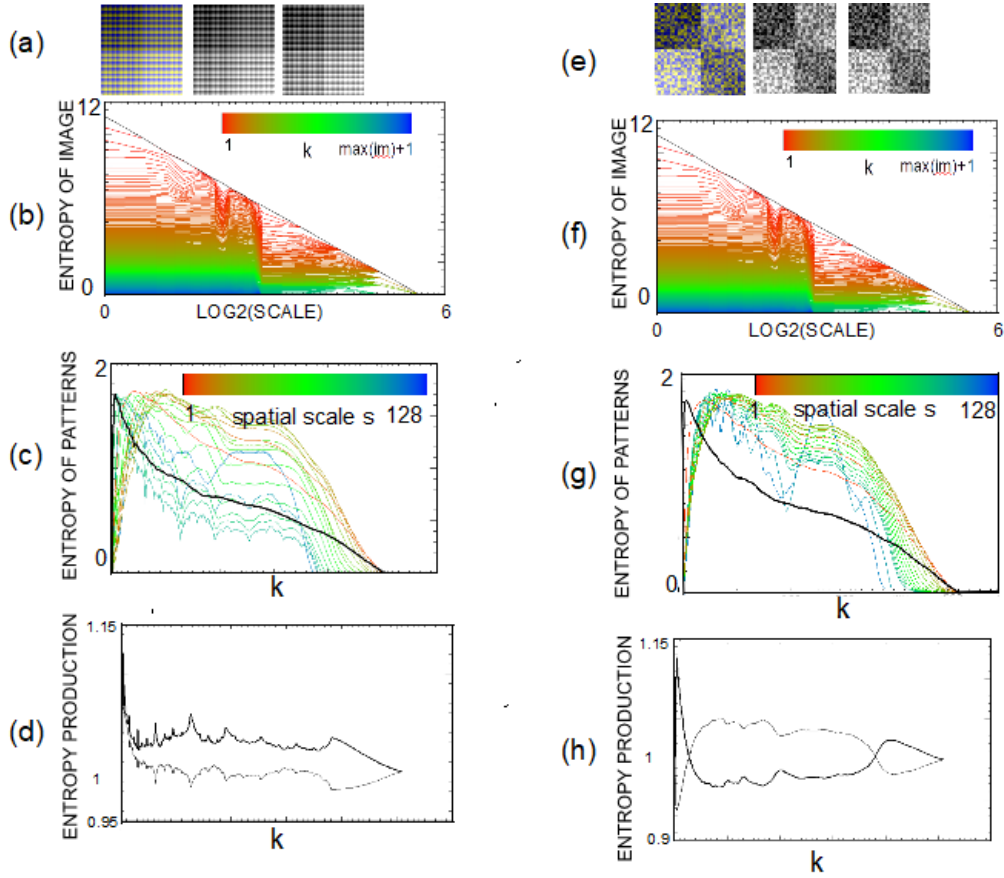


Fig. 16. Modified Hilbert Fractal FCI ($256 \times 256 \times 2$ channels, dynamics 2^*N) best fit the three laws. Randomness in the angle of rotation of the Hilbert 2×2 0123 pattern (top) allows for a better fit of pattern entropy and a more accurately balanced entropy production than regular pattern (bottom). snapshots: Image 2 channels (Left) green-red, (Middle) channel1, (Right) channel2.

5. Conclusion

Patterns can be distinguished, ordered and eventually valued. General studies of natural images relying on analogies to physical model assumes patterns with assigned values. Based on the weakest assumption of distinguishable patterns, we observe in this study three universal laws of natural images associated to scales and dynamics. This work may inspire advancements in neural networks-based image analysis. In particular, the design and training of these networks may benefit from the three reported universal observations about images of natural scenes. The study also offers a context of physical complex phenomena, as log-scale laws (L1) and entropy fluctuation (L3) in images have analogs in physics of chaotic systems. We did not find in physics an equivalent of the law L2 about an universal value of the entropy, reached at some dynamics, of a local Hamiltonian of interaction. We propose that optimal settings of recorders should offer dynamics and channels capable of capturing fully colored images of studied scenes. Furthermore, this study provides a combinatorial perspective on natural scenes, depicting them as sets of fully colored tiles adhering to three universal multi-scale combinatorial constraints regarding their partitioning into the 2D puzzle-image.

Acknowledgments. This study benefited from short yet invaluable discussions with Oriol Bohigas, Christian Lavault and Henning Bruhn-Fujimoto.

Data availability. Data underlying the results presented in this paper are available in Ref. [39–41, 49, 51].

References

1. Geoffrey J Burton and Ian R Moorhead. Color and spatial structure in natural scenes. *Applied optics*, 26(1):157–170, 1987.
2. Daniel L Ruderman and William Bialek. Statistics of natural images: Scaling in the woods. *Physical review letters*, 73(6):814, 1994.
3. Anuj Srivastava, Ann B Lee, Eero P Simoncelli, and S-C Zhu. On advances in statistical modeling of natural images. *Journal of mathematical imaging and vision*, 18:17–33, 2003.
4. Maria Zontak and Michal Irani. Internal statistics of a single natural image. In *CVPR 2011*, pages 977–984. IEEE, 2011.
5. Saeed Saremi and Terrence J Sejnowski. Hierarchical model of natural images and the origin of scale invariance. *Proceedings of the National Academy of Sciences*, 110(8):3071–3076, 2013.
6. Michelle M Roberts, Mark M Schira, Branka Spehar, and Zoey J Isherwood. Nature in motion: the tuning of the visual system to the spatiotemporal properties of natural scenes. *Journal of Vision*, 22(6):7–7, 2022.
7. Donald L Turcotte. *Fractals and chaos in geology and geophysics*. Cambridge university press, 1997.
8. PR Renosh, Francois G Schmitt, and Hubert Loisel. Scaling analysis of ocean surface turbulent heterogeneities from satellite remote sensing: use of 2d structure functions. *PLoS one*, 10(5):e0126975, 2015.
9. Michael C Roggemann and Byron M Welsh. *Imaging through turbulence*. CRC press, 2018.
10. Federico Corberi, Leticia F Cugliandolo, Marco Esposito, Onofrio Mazzarisi, and Marco Picco. How many phases nucleate in the bidimensional potts model? *Journal of Statistical Mechanics: Theory and Experiment*, 2022(7):073204, 2022.
11. Daniel Glasner, Shai Bagon, and Michal Irani. Super-resolution from a single image. In *2009 IEEE 12th international conference on computer vision*, pages 349–356. IEEE, 2009.
12. Matthew D Zeiler and Rob Fergus. Visualizing and understanding convolutional networks. In *Computer Vision—ECCV 2014: 13th European Conference, Zurich, Switzerland, September 6–12, 2014, Proceedings, Part I 13*, pages 818–833. Springer, 2014.
13. Marvin S Keshner. $1/f$ noise. *Proceedings of the IEEE*, 70(3):212–218, 1982.
14. Daniel L Ruderman. Origins of scaling in natural images. *Vision research*, 37(23):3385–3398, 1997.
15. Yanguang Chen. Zipf’s law, $1/f$ noise, and fractal hierarchy. *Chaos, Solitons & Fractals*, 45(1):63–73, 2012.
16. Andrey A Bagrov, Ilia A Iakovlev, Askar A Iliasov, Mikhail I Katsnelson, and Vladimir V Mazurenko. Multiscale structural complexity of natural patterns. *Proceedings of the National Academy of Sciences*, 117(48):30241–30251, 2020.
17. Tim Herpich and Massimiliano Esposito. Universality in driven potts models. *Physical Review E*, 99(2):022135, 2019.
18. Christopher Jarzynski. Nonequilibrium equality for free energy differences. *Physical Review Letters*, 78(14):2690, 1997.
19. Giuseppe Boccignone and Mario Ferraro. Entropy production in colour images. In *Proceedings 15th International Conference on Pattern Recognition. ICPR-2000*, volume 1, pages 202–205. IEEE, 2000.
20. Giuseppe Boccignone, M Ferrearo, and Terry Caelli. Encoding visual information using anisotropic transformations. *IEEE Transactions on Pattern Analysis and Machine Intelligence*, 23(2):207–211, 2001.
21. Mario Ferraro, Giuseppe Boccignone, and Terry Caelli. Entropy-based representation of image information. *Pattern Recognition Letters*, 23(12):1391–1398, 2002.
22. Mario Ferraro and Giuseppe Boccignone. Image contrast enhancement via entropy production. *Real-Time Imaging*, 10(4):229–238, 2004.
23. Udo Seifert. Stochastic thermodynamics, fluctuation theorems and molecular machines. *Reports on progress in physics*, 75(12):126001, 2012.
24. Luca Cocconi, Guillaume Salbreux, and Gunnar Pruessner. Scaling of entropy production under coarse graining in active disordered media. *Physical Review E*, 105(4):L042601, 2022.
25. Gregory W Wornell. Wavelet-based representations for the $1/f$ family of fractal processes. *Proceedings of the IEEE*, 81(10):1428–1450, 1993.
26. Timo Ojala, Matti Pietikainen, and Topi Maenpaa. Multiresolution gray-scale and rotation invariant texture classification with local binary patterns. *IEEE Transactions on pattern analysis and machine intelligence*, 24(7):971–987, 2002.
27. Yanshan Li, Haojin Tang, Weixin Xie, and Wenhan Luo. Multidimensional local binary pattern for hyperspectral image classification. *IEEE Transactions on Geoscience and Remote Sensing*, 60:1–13, 2021.
28. Ibrahim M Alabdulmohsin, Behnam Neyshabur, and Xiaohua Zhai. Revisiting neural scaling laws in language and vision. *Advances in Neural Information Processing Systems*, 35:22300–22312, 2022.
29. Matteo Marsili and Yasser Roudi. Quantifying relevance in learning and inference. *Physics Reports*, 963:1–43, 2022.

30. Zoey J Isherwood, Mark M Schira, and Branka Spehar. The tuning of human visual cortex to variations in the $1/f\alpha$ amplitude spectra and fractal properties of synthetic noise images. *Neuroimage*, 146:642–657, 2017.
31. Stefan Thurner, Rudolf Hanel, and Peter Klimek. *Introduction to the theory of complex systems*. Oxford University Press, 2018.
32. Jared Kaplan, Sam McCandlish, Tom Henighan, Tom B Brown, Benjamin Chess, Rewon Child, Scott Gray, Alec Radford, Jeffrey Wu, and Dario Amodei. Scaling laws for neural language models. *arXiv preprint arXiv:2001.08361*, 2020.
33. Xu-Wen Wang and Yang-Yu Liu. Origins of scaling laws in microbial dynamics. *Physical Review Research*, 5(1):013004, 2023.
34. Greg J Stephens, Thierry Mora, Gašper Tkačik, and William Bialek. Statistical thermodynamics of natural images. *Physical review letters*, 110(1):018701, 2013.
35. Saeed Saremi and Terrence J Sejnowski. On criticality in high-dimensional data. *Neural computation*, 26(7):1329–1339, 2014.
36. Saeed Saremi and Terrence J Sejnowski. The wilson machine for image modeling. *arXiv preprint arXiv:1510.07740*, 2015.
37. Saeed Saremi and Terrence J Sejnowski. Correlated percolation, fractal structures, and scale-invariant distribution of clusters in natural images. *IEEE transactions on pattern analysis and machine intelligence*, 38(5):1016–1020, 2015.
38. Tomoyuki Obuchi, Hirokazu Koma, and Muneki Yasuda. Boltzmann-machine learning of prior distributions of binarized natural images. *Journal of the Physical Society of Japan*, 85(11):114803, 2016.
39. David H Foster, Kinjiro Amano, Sérgio MC Nascimento, and Michael J Foster. Frequency of metamerism in natural scenes. *Josa a*, 23(10):2359–2372, 2006.
40. Yusukex Monno, Sunao Kikuchi, Masayuki Tanaka, and Masatoshi Okutomi. A practical one-shot multispectral imaging system using a single image sensor. *IEEE Transactions on Image Processing*, 24(10):3048–3059, 2015.
41. Seonghyeon Nam, Seoung Wug Oh, Jae Yeon Kang, Chang Ha Shin, Younghyun Jo, Young Hwi Kim, Kyungmin Kim, Minh Shim, Sungho Lee, Yunji Kim, Suho Han, Gunhee Nam, Dasol Lee, Subin Jeon, In Cho, Woongoh Cho, Sejong Yang, Dongyoung Kim, Hyolim Kang, Sukjun Hwang, and Seon Joo Kim. Real and fake face detection, version 1. <https://www.kaggle.com/datasets/ciplab/real-and-fake-face-detection>, 2019. Accessed: June 13, 2024.
42. van der Arjen Schaaf and van Johannes Hateren. Modelling the power spectra of natural images: Statistics and information. *Vision Research*, 36:2759–2770, 1996.
43. Alexandros Alexakis and Luca Biferale. Cascades and transitions in turbulent flows. *Physics Reports*, 767:1–101, 2018.
44. Leonid M Martyushev and Vladimir D Seleznev. Maximum entropy production principle in physics, chemistry and biology. *Physics reports*, 426(1):1–45, 2006.
45. A Kondi, V Constantoudis, P Sarkiris, K Ellinas, and E Gogolides. Using chaotic dynamics to characterize the complexity of rough surfaces. *Physical Review E*, 107(1):014206, 2023.
46. Per Bak, Chao Tang, and Kurt Wiesenfeld. Self-organized criticality. *Physical review A*, 38(1):364, 1988.
47. John M Beggs and Dietmar Plenz. Neuronal avalanches in neocortical circuits. *Journal of neuroscience*, 23(35):11167–11177, 2003.
48. Beatrice Pesquet-Popescu and Jacques Lévy Véhel. Stochastic fractal models for image processing. *IEEE signal processing magazine*, 19(5):48–62, 2002.
49. GTOPO30. Dem. <https://rda.ucar.edu/datasets/ds758.0/>. Accessed: June 13, 2024.
50. Chao Dong, Chen Change Loy, Kaiming He, and Xiaoou Tang. Image super-resolution using deep convolutional networks. *IEEE transactions on pattern analysis and machine intelligence*, 38(2):295–307, 2015.
51. DeepAI. DeepAI - torch-srgan. <https://deepai.org/machine-learning-model/torch-srgan>. Accessed: June 13, 2024.